



HAL
open science

Methodologies to assess mean annual air pollution concentration combining numerical results and wind roses

Nicolas Reiminger, Xavier Jurado, José Vazquez, Cédric Wemmert, Nadège Blond, Jonathan Wertel, Matthieu Dufresne

► To cite this version:

Nicolas Reiminger, Xavier Jurado, José Vazquez, Cédric Wemmert, Nadège Blond, et al.. Methodologies to assess mean annual air pollution concentration combining numerical results and wind roses. *Sustainable Cities and Society*, 2020, 59, pp.102221. 10.1016/j.scs.2020.102221 . hal-03051698

HAL Id: hal-03051698

<https://hal.science/hal-03051698>

Submitted on 10 Dec 2020

HAL is a multi-disciplinary open access archive for the deposit and dissemination of scientific research documents, whether they are published or not. The documents may come from teaching and research institutions in France or abroad, or from public or private research centers.

L'archive ouverte pluridisciplinaire **HAL**, est destinée au dépôt et à la diffusion de documents scientifiques de niveau recherche, publiés ou non, émanant des établissements d'enseignement et de recherche français ou étrangers, des laboratoires publics ou privés.

See discussions, stats, and author profiles for this publication at: <https://www.researchgate.net/publication/341035519>

Methodologies to assess mean annual air pollution concentration combining numerical results and wind roses

Article in *Sustainable Cities and Society* · April 2020

DOI: 10.1016/j.scs.2020.102221

CITATION

1

READS

79

7 authors, including:



Nicolas Reiminger

AIR&D

8 PUBLICATIONS 8 CITATIONS

[SEE PROFILE](#)



Xavier Jurado

ICube Laboratory

4 PUBLICATIONS 5 CITATIONS

[SEE PROFILE](#)



José Vazquez

Ecole Nationale du Génie de l'Eau et de l'Environnement de Strasbourg

133 PUBLICATIONS 584 CITATIONS

[SEE PROFILE](#)



Cédric Wemmert

University of Strasbourg

86 PUBLICATIONS 840 CITATIONS

[SEE PROFILE](#)

Some of the authors of this publication are also working on these related projects:



3D Modelling of Air Pollution at Urban Scale - Ph.D. thesis [View project](#)



COCLICO (ANR Project) [View project](#)

1 Methodologies to assess mean annual air pollution concentration combining 2 numerical results and wind roses

3 Nicolas Reiminger^{1,2†*}, Xavier Jurado^{1,2*}, José Vazquez², Cédric Wemmert², Nadège Blond³,
4 Jonathan Wertel¹, Matthieu Dufresne¹

5 ¹AIR&D, 67000, Strasbourg, France

6 ²ICUBE Laboratory, CNRS/University of Strasbourg, 67000, Strasbourg, France

7 ³LIVE Laboratory, CNRS/University of Strasbourg, 67000, Strasbourg, France

8 [†]Corresponding author: Tel. +33 (0)6 31 26 75 88, Mail. nreiminger@air-d.fr

9 ^{*}These authors contributed equally to this work

10

11 Please cite this paper as : Reiminger, N., Jurado, X., Vazquez, J., Wemmert, C., Dufresne, M., Blond,
12 N., Wertel, J., 2020. Methodologies to assess mean annual air pollution concentration combining
13 numerical results and wind roses. Sustainable Cities and Society, 59,
14 102221. DOI: 1016/j.scs.2020.102221

15

16 ABSTRACT

17 Numerical models are valuable tools to assess air pollutant concentrations in cities which can
18 be used to define new strategies to achieve sustainable cities of the future in terms of air quality.
19 Numerical results are however difficult to be directly compared to air quality standards since
20 they are usually valid only for specific wind speed and direction while some standards are on
21 annual values. The purpose of this paper is to present existing and new methodologies to turn
22 numerical results into mean annual concentrations and discuss their limitations. To this end,
23 methodologies to assess wind speed distribution based on wind rose data are presented first.
24 Then, methodologies are compared to assess mean annual concentrations based on numerical
25 results and on wind speed distributions. According to the results, a Weibull distribution can be
26 used to accurately assess wind speed distribution in France, but the results can be improved
27 using a sigmoid function presented in this paper. It is also shown that using the wind rose data
28 directly to assess mean annual concentrations can lead to underestimations of annual
29 concentrations. Finally, the limitations of discrete methodologies to assess mean annual
30 concentrations are discussed and a new methodology using continuous functions is described.

31

32 **1. Introduction**

33 Over the past decades, outdoor air pollution has become a major issue, especially in highly
34 densified urban areas where pollutant sources are numerous and air pollutant emissions high.
35 In order to protect people from excessive exposure to air pollution, which can cause several
36 diseases (Anderson et al., 2012; Kim et al., 2015), the World Health Organization (WHO) have
37 recommended standard values that must not be exceeded for different pollutants such as
38 nitrogen dioxide (NO₂) and particulate matter (EU, 2008; WHO, 2017) to protect population
39 health, and the European Union (EU) decided to respect the same or other standards depending
40 on the air pollutants. Among the different types of values given as standards, studies have
41 shown that annual standards are generally more constraining and harder to reach than the other
42 standards (Chaloulakou et al., 2008; Jenkin, 2004).

43 In the meantime, recent studies have shown that the indoor air quality is strongly correlated
44 with the outdoor one: while for nitrogen dioxide a 5% increase in indoor air pollutant
45 concentrations can be expected for only a 1% increase in outdoor concentrations (Shaw et al.,
46 2020), for particulate matters such as PM_{2.5} the outdoor concentration can contribute from 27%
47 to 65% of the indoor concentration (Bai et al., 2020). Being able to assess outdoor pollutant
48 concentrations is therefore a necessity to improve air quality in the outdoor built environment,
49 but also in the indoor one (Scibor et al., 2019).

50 Annual concentrations can be assessed using both on-site monitoring and numerical modeling.

51 On site monitoring requires measurements over long periods to be able to assess mean annual
52 concentrations of pollutants, although a recent study has shown that mean annual concentration
53 of NO₂ can be assessed using only one month of data (Jurado et al., 2020), which significantly
54 reduces the measurement time required. Monitoring nonetheless has other limitations: it does
55 not allow assessing the future evolution of the built environment or pollutant emissions, thus,

56 limiting its applicability to achieve the smart sustainable cities of the future as defined by Bibri
57 and Krogstie (2017). Numerical modelling can overcome these limitations and can help define
58 new strategies to improve air quality in cities combining wind data, various air pollution
59 scenarios and urban morphologies (Yang et al., 2020). Among the several models currently
60 available, Computational Fluid Dynamics (CFD) has shown great potential for modeling
61 pollutant dispersion from traffic-induced emissions by including numerous physical
62 phenomena such as the effects of trees (Buccolieri et al., 2018; Santiago et al., 2019; Vranckx
63 et al., 2015) and heat exchanges (Qu et al., 2012; Toparlar et al., 2017; Wang et al., 2011) on
64 the scale of a neighborhood. However, this type of numerical result cannot be directly compared
65 with the annual standards. Methodologies designed to assess mean annual concentrations based
66 on numerical results, such as described by Solazzo et al. (2011), are thus required and further
67 work is required to improve these methodologies and assess their limits.

68 The aim of this study is to provide tools and methodologies to assess mean annual
69 concentrations based on numerical results and wind rose data to improve air quality in built
70 environment and cities. It is firstly to evaluate whether it is possible to assess continuous wind
71 speed distributions based on wind rose data. To do so, a statistical law called Weibull
72 distribution is compared with a new sigmoid-based function built for the purpose of this study.
73 Secondly, it is to present and compare a discrete methodology usually used to assess mean
74 annual concentrations based on numerical results with a continuous methodology built for the
75 purpose of this study, and to discuss their respective advantages and limitations. The data used
76 for the wind speed distribution assessments, the area modeled and the CFD model used for
77 illustration purposes are presented in Section 2. Then, the description and the comparison of
78 the different methodologies are presented in Section 3 and, finally, a discussion is provided in
79 Section 4.

80

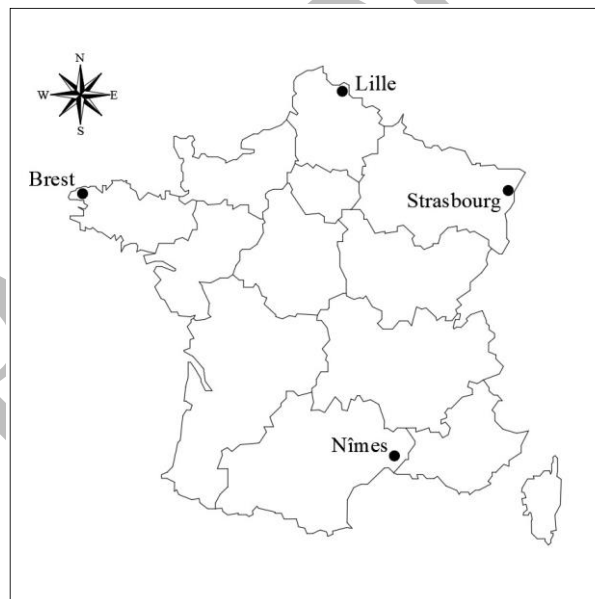
81

82 2. Material and methods

83 2.1. Meteorological data

84 2.1.1. Data location

85 This work uses wind velocity and wind direction data from four cities in France. These cities
86 were chosen to cover most of France to obtain representative results and include the cities of
87 Strasbourg (Grand-Est region), Nîmes (Occitanie region), Brest (Bretagne region) and Lille
88 (Hauts-de-France region). In particular, the data were obtained from the stations named
89 Strasbourg-Entzheim, Nîmes-Courbessac, Brest-Guipavas and Lille-Lesquin, respectively. The
90 location of these stations and their corresponding regions are presented in Fig. 1.



91

92 Fig. 1. Location of the different meteorological stations used.

93 2.1.2. Data availability and data range

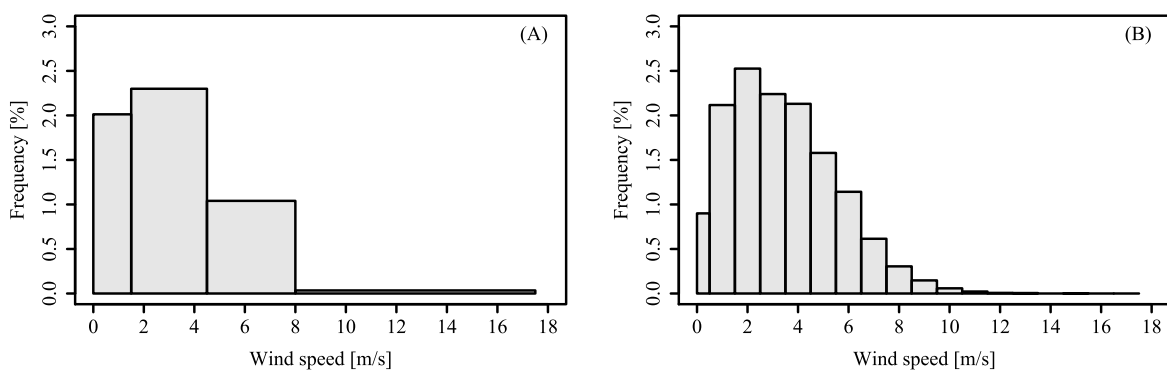
94 The data used in this work were provided by Météo-France, a public institution and France's
95 official meteorology and climatology service. The data are mainly couples of wind velocity and
96 wind direction over a twenty-year period from 1999 to 2018, except for the Strasbourg-

97 Entzheim station where it is a ten-year period from 1999 to 2008. The data were obtained via a
 98 personal request addressed to Météo-France and were not available on open-access. A summary
 99 of the information of the stations is presented in Table 1, with the time ranges of the data and
 100 the number of data available (the coordinates are given in the World Geodetic System 1984).

101 Table 1. Summary of the available data.

Location	Station			Data availability		
	Latitude	Longitude	Altitude	Time range	Number of valid cases	Number of missing cases
Brest - Guipavas	48°27'00"N	4°22'59"O	94 m	2009 - 2018	29,171	45
Lille - Lesquin	50°34'12"N	3°05'51"E	47 m	2009 - 2018	29,185	31
Nîmes - Courbessac	43°51'24"N	4°24'22"E	59 m	2009 - 2018	29,214	2
Strasbourg - Entzheim	48°32'58"N	7°38'25"E	150 m	1999 - 2008	29,199	25

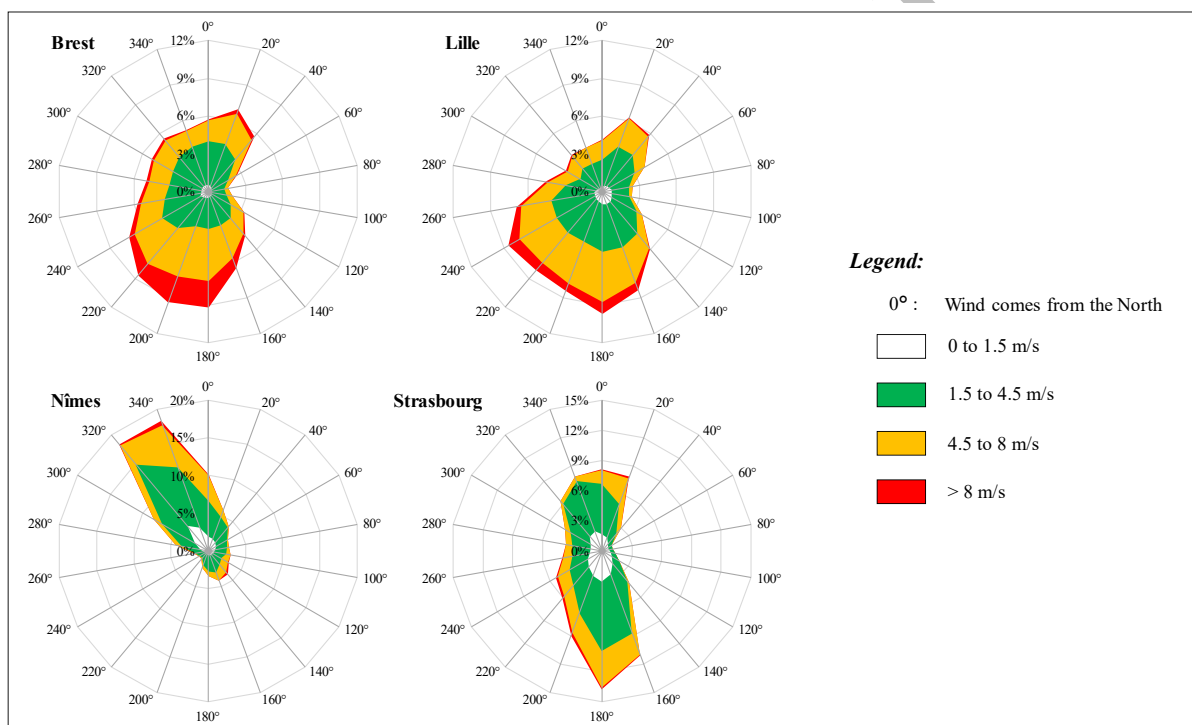
102
 103 All the data were monitored from wind sensors placed 10 meters from the ground and the wind
 104 frequencies are available for each wind direction with 20° steps for two distinct wind
 105 discretizations: a “basic” discretization giving wind frequencies for 4 velocity ranges (from 0
 106 to 1.5 m/s, 1.5 to 3.5 m/s, 3.5 to 8 m/s and more than 8 m/s), illustrated in Fig. 2. (A); and a
 107 “detailed” discretization giving wind frequencies by 1 m/s steps except between 0 and 0.5 m/s,
 108 illustrated in Fig. 2. (B). The “basic” discretization is a common format mostly found in wind
 109 roses (possibly with different velocity ranges) while the “detailed” data are less common and
 110 more expensive.



111

112 Fig. 2. Example of data for Strasbourg and a 200° wind direction with (A) only 4 ranges of velocities and (B) the detailed
 113 data discretized in 18 ranges.

114 The wind roses for each meteorological station considered in this work and based on the “basic”
 115 4-velocity-range discretization described in Fig. 2. (A) are provided in Fig. 3. This figure shows
 116 how the monitoring locations considered in this study give distinct but complementary
 117 information, with for example many high velocities at Brest compared to Strasbourg and Nîmes,
 118 where almost no velocities were monitored over 8 m/s, and with dominant wind directions at
 119 Nîmes and Strasbourg compared to the other stations.



120

121

Fig. 3. Wind roses for each location considered.

122

123 2.1.3. Interpolation functions

124 A two-parametric continuous probability function, the Weibull distribution, mainly used in the
 125 wind power industry, can be used to describe wind speed distribution (Kumar et al., 2019;

126 Mahmood et al., 2019). The equation of the corresponding probability density function is given
 127 in (1).

$$128 \quad f(v) = \frac{k}{\lambda} \left(\frac{v}{\lambda}\right)^{k-1} e^{-(v/\lambda)^k} \quad (1)$$

129 where v is the wind velocity, k is the shape parameter and λ is the scale parameter of the
 130 distribution, with k and λ being positive.

131 For the purpose of this study, an original 5-parametric continuous function was built to
 132 determine the “detailed” wind discretization based on the “basic” 4-velocity-range wind
 133 discretization. This function, called Sigmoid function, based on the composition of two sigmoid
 134 functions, is given in (2). The two functions will be compared in the results section.

$$135 \quad f(v) = \alpha \cdot \left(-1 + \frac{1}{1 + \beta_1 \cdot e^{-\gamma_1 \cdot v}} + \frac{1}{1 + \beta_2 \cdot e^{\gamma_2 \cdot v}} \right) \quad (2)$$

136 where α , β_1 , β_2 , γ_1 and γ_2 are positive parameters.

138 2.2. Numerical model

139 Simulations were performed using the unsteady and incompressible solver *pimpleFoam* from
 140 OpenFOAM 6.0. A Reynolds-Averaged Navier-Stokes (RANS) methodology was used to solve
 141 the Navier-Stokes equations with the RNG k- ϵ turbulence model, and the transport of
 142 particulate matter was performed using a transport equation. This solver was validated
 143 previously in Reiminger et al. (2020).

144 The area chosen to illustrate the methodologies discussed in this paper is located in
 145 Schiltigheim, France (48°36'24", 7°44'00"), a few kilometers north of Strasbourg. This area, as
 146 well as the only road considered as an emission source in this study (D120, rue de la Paix), are
 147 illustrated in Fig. 4. (A). PM₁₀ traffic-related emissions were estimated at 1.39 mg/s using daily

148 annual mean traffic and were applied along the street considering its length in the numerical
 149 domain (200 m), its width (9 m) and an emission height of 0.5 m to take into account initial
 150 dispersion.

151 The recommendations given by Franke et al. (2007) were followed. In particular, with H being
 152 the highest building height (16 m), the distances between the buildings and the lateral
 153 boundaries are at least $5H$, the distances between the inlet and the buildings as well as for the
 154 outlet and the buildings are at least $5H$ and the domain height is around $6H$. An illustration of
 155 the resulting 3D sketch is presented in Fig. 4. (B). A grid sensitivity test was performed and
 156 showed that hexahedral meshes of 1 m in the study area and 0.5 m near the building walls are
 157 sufficient, leading to a more comparable resolution than other CFD studies (Blocken, 2015) and
 158 leading to a total number of around 800,000 cells. The resulting mesh is illustrated in Fig. 5.



159
 160 Fig. 4. Illustration of (A) the area of Strasbourg modeled with the road considered for the traffic-related emissions (white
 161 dashed lines), and (B) the corresponding area built in 3D for the numerical simulations with the emission source (red).

162

163 No-slip conditions ($U = 0$ m/s) were applied to the building walls and ground, and symmetry
 164 conditions to the lateral and the top boundaries. A freestream condition was applied to the outlet
 165 boundary, and neutral velocity, turbulent kinetic energy and turbulent dissipation profiles
 166 suggested by Richards and Norris (2011) were applied to the inlet boundary.

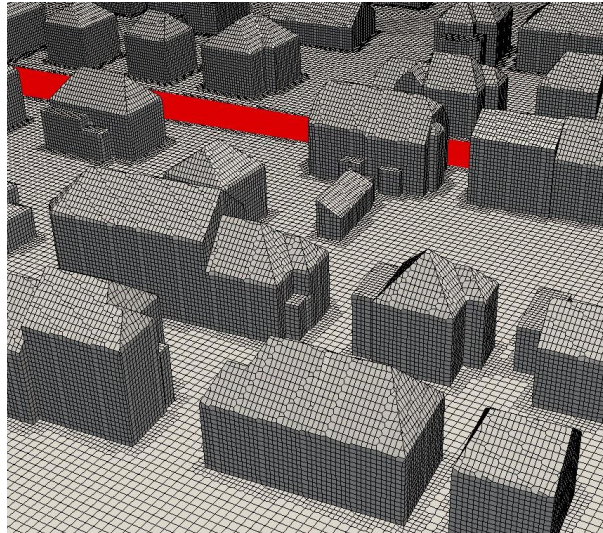
167 A total of 18 simulations were performed using the same wind velocity ($U_{10m} = 1.5$ m/s) but
 168 with different wind directions from 0° to 340° using a 20° step. Since the simulations were
 169 performed in neutral conditions and without traffic-induced turbulence, the dimensionless
 170 concentration C^* given in (3) is a function only of the wind direction (Schatzmann and Leitl,
 171 2011). In other words, this means that considering the previous hypothesis, and for a given
 172 emission and building configuration (leading to constant $H \cdot L/q$ ratio), only one simulation is
 173 needed for each wind direction simulated. The pollutant concentrations for a non-simulated
 174 wind velocity u can therefore be computed using (4).

$$175 \quad C^* = \frac{C \cdot U \cdot H \cdot L}{q} \quad (3)$$

176 where C^* is the dimensionless concentration, C is the concentration, U the wind velocity, H
 177 the characteristic building height and q/L the source strength of emission.

$$178 \quad C_u = U_{ref} \cdot \frac{C_{ref}}{u} \quad (4)$$

179 where C_u is the pollutant concentration for the wind velocity u not simulated and C_{ref} the
 180 pollutant concentration for the simulated wind velocity U_{ref} .



181

182

183

Fig. 5. Illustration of the meshes in the computational domain with the emission source (red), with 0.5 m meshes near the buildings and 1 m in the study area.

184

3. Results

185

3.1. Wind data interpolation

186

3.1.1. Comparison between the Weibull distribution and the sigmoid function

187

188

189

190

191

192

193

194

195

The best fitting parameters of the two functions were determined for the whole dataset using a non-linear solver and the “basic” 4-velocity-range wind data. The solver was set up to solve equation (5) for the four-velocity ranges $[0, 1.5[$, $[1.5, 4.5[$, $[4.5, 8[$ and $[8, +\infty[$ for both the Weibull and the sigmoid functions. This equation reflects that the sum of the frequencies between two wind velocities (i.e. the area under the curve) must be equal to the frequency given in the “basic” 4-velocity-range wind data. Since the sigmoid function has five parameters, a fifth equation to be solved was added only for this function and corresponds to (6). With this equation, it is assumed that the wind frequency tends toward 0% when the wind speed tends toward 0 m/s, as for the Weibull distribution.

196

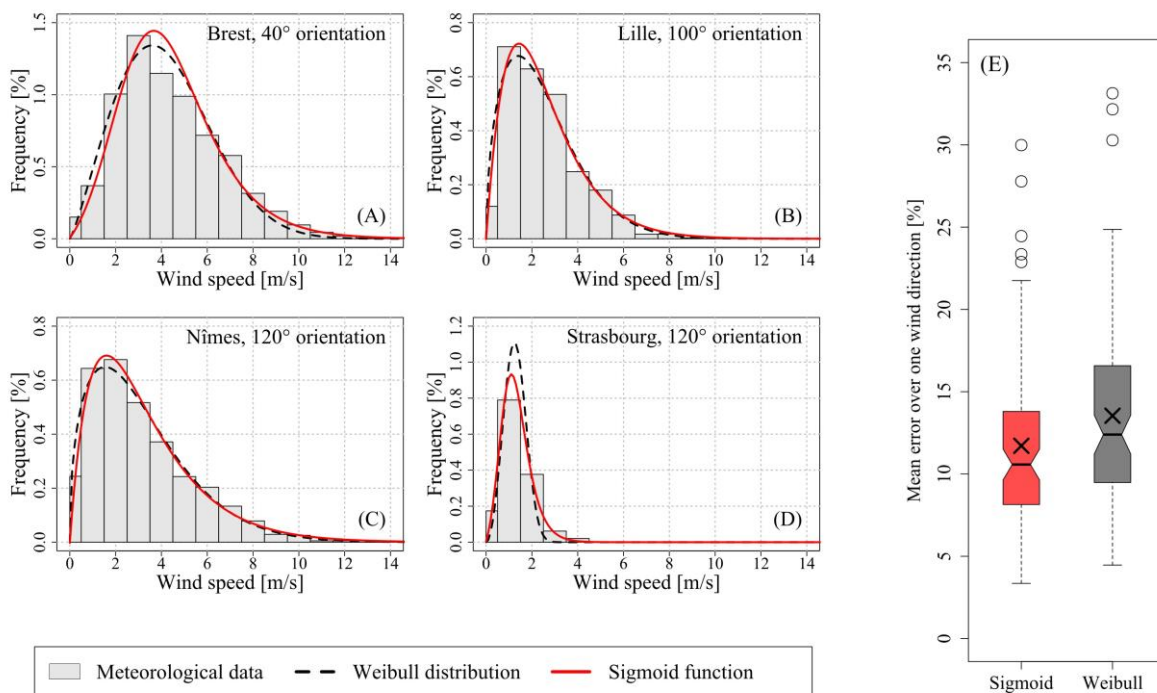
$$\int_a^b f(v) \cdot dv = FVR_{[a,b[} \quad (5)$$

197

$$f(0) = 0 \quad (6)$$

198 where $f(v)$ is the Weibull or the sigmoid function and $FVR_{[a;b]}$ is the wind frequency given in
 199 the 4-velocity-range data for wind velocities ranging from a included to b excluded.

200 Fig. 6 (A–D) shows a comparison between the Weibull distribution, the sigmoid function and
 201 the “detailed” 18-velocity-range data for one wind direction of each meteorological station.
 202 According to these figures, the two functions generally give the same trends, and both appear
 203 to give a good estimation of the “detailed” wind data. However, depending on the case, the
 204 Weibull function can provide improvements in comparison to the sigmoid function, as in Fig.
 205 6. (A), or vice versa, the sigmoid function can provide improvements in comparison to the
 206 Weibull function, as in Fig. 6. (D).



207
 208 Fig. 6. (A–D) Weibull distribution and sigmoid function results compared to the detailed meteorological wind frequency data
 209 for one wind direction at each station considered and (E) a notched box plot of the mean error over one wind direction with
 210 all stations included for both functions.

211 To better compare the two functions, a notched box plot of the mean error over one wind
 212 direction is given in Fig. 6. (E). According to this figure, the sigmoid function gives generally
 213 better results compared to the Weibull distribution, with a lower maximal error (30.0% and

214 33.1% respectively); a lower first quartile (8.1% and 9.5% resp.); a lower third quartile (13.8%
215 and 14.5% resp.); a lower mean (11.7% and 13.5% resp.); and a lower median (10.6% and
216 12.4% resp.). The differences are, however, small and may not be significant, especially for the
217 median because the notches slightly overlap. These differences between the Weibull
218 distribution and the sigmoid function are also location dependent, with for example better
219 prediction of the wind distribution in Strasbourg using the sigmoid function and an equivalent
220 prediction in Brest. Finally, it should be noted that both functions can lead to underestimations
221 of the lower wind velocity frequencies, as shown in Fig. 6. (A) and (D).

222 According to the previous results, the Weibull distribution and the sigmoid function can
223 accurately reproduce the “detailed” wind distribution based on a “basic” 4-velocity-range
224 discretization with an average error of around 12% over the four stations considered in France.
225 They can nonetheless lead to underestimations of the low wind velocity frequencies, for which
226 the highest pollutant concentrations appear.

227

228 *3.1.2. Optimization of the sigmoid function interpolation for low wind velocities*

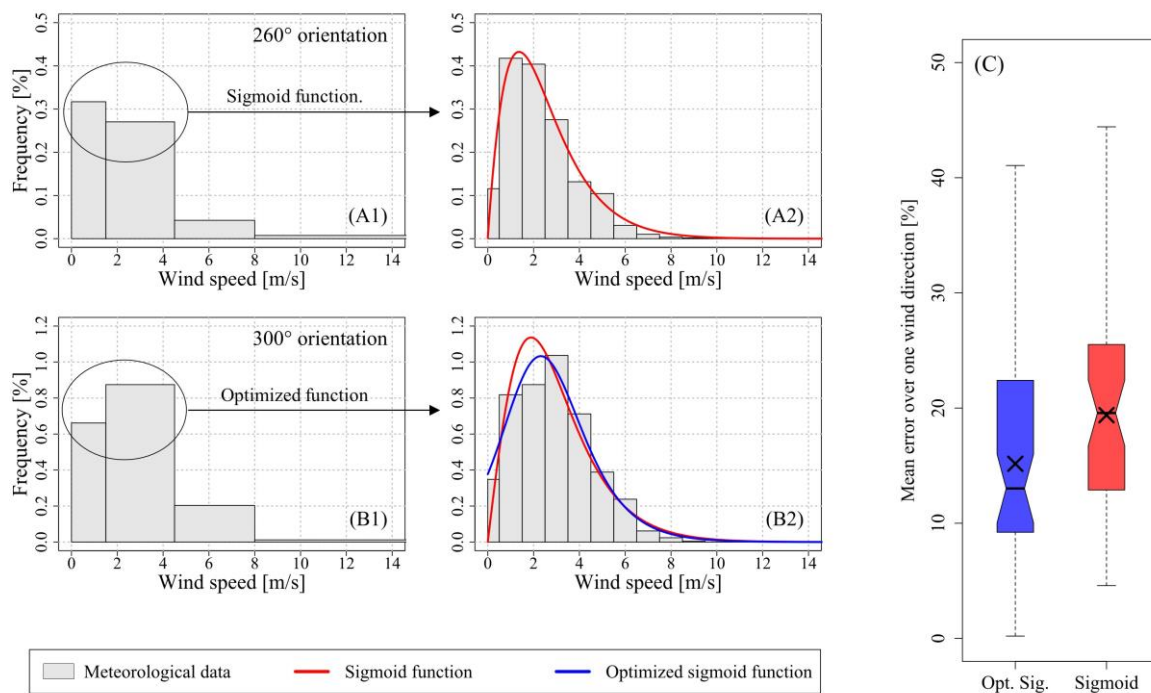
229 The parametrization of the sigmoid function, called standard sigmoid function, was modified
230 to improve the estimation of the low wind velocity frequencies in order to avoid
231 underestimating pollutant concentrations.

232 Based on all the meteorological data considered in this study, it was found that the
233 underestimation of low wind velocity frequencies occurs mostly when the frequency of the first
234 velocity range is lower than the frequency of the second velocity range. In this specific case,
235 the optimized sigmoid function still needs the equation (5) for the four-velocity ranges given in
236 the “basic” wind data, but equation (6) is replaced by equation (7); otherwise, the previous
237 parametrization using equations (5) and (6) is kept.

$$f(0) = FVR_{[0;\alpha[} \frac{FVR_{[0,\alpha[}}{FVR_{[\alpha,\beta[}} \quad (7)$$

238 where $FVR_{[0,\alpha[}$ is the wind frequency for the first range of velocities given in the 4-velocity-
 239 range data and $FVR_{[\alpha,\beta[}$ is the wind frequency for the second range of velocities (e.g., in this
 240 study $\alpha = 1.5$ and $\beta = 4.5$).
 241

242 The methodology for the optimized sigmoid function is illustrated in Fig. 7. (A–B): when the
 243 frequency of the first velocity range is higher than the second, as in Fig. 7. (A1), the standard
 244 parametrization of the sigmoid function can be used because the low wind velocity frequencies
 245 are estimated accurately, as in Fig. 7. (A2), when the frequency of the first velocity range is
 246 lower than the second, as in Fig. 7. (B1), the standard parametrization leads to underestimations
 247 of low wind velocity frequencies and the optimized parametrization should be used instead,
 248 leading to a better estimation of the frequencies, as shown by the blue curve in Fig. 7. (B2)
 249 compared to the red curve.



250

251 Fig. 7. (A–B) Illustration of the optimized sigmoid function methodology and (C) comparison with the standard sigmoid

252

function results.

253 The improvements with the optimized sigmoid function compared to the standard function were
254 assessed and the results are presented in Fig. 7. (C). For this comparison, only the wind
255 directions where the optimized function was applied are considered and the errors compared to
256 the “detailed” 18-velocity-range data were calculated for the low wind velocity frequencies
257 (between 0 and 3.5 m/s). According to this figure, the optimized sigmoid function gives
258 improvements over the standard sigmoid function with a lower maximal error (41.0% and
259 44.4% respectively); a lower first quartile (9.2% and 12.9% resp.); a lower third quartile (22.4%
260 and 25.5% resp.); a lower mean error (15.2% and 19.4% resp.); and a lower median (13.0% and
261 19.6% resp.). The improvements using the optimized function are significant, in particular for
262 the median since the box plot notches do not overlap; they are also location dependent. A global
263 improvement of the wind distribution prediction ranging between 20% and 45% is observed in
264 Strasbourg, Lille and Nîmes while no improvement is observed in Brest.

265 According to the previous results, using the optimized sigmoid function can improve the
266 reproduction of the “detailed” wind distribution based on a “basic” 4-velocity-range compared
267 to the standard sigmoid function, especially for low wind velocities.

268 3.2. Mean annual concentration assessment

269 3.2.1. Discrete methodology with intermediate velocities

270 Initially, mean annual concentrations based on the CFD results can be calculated using a
271 discrete methodology. This methodology considers that the mean annual concentration at a
272 given location is composed of several small contributions of different wind velocities and wind
273 directions. The mean concentration over one wind direction can be calculated with equation (8)
274 and the mean annual concentration with equation (9). A similar methodology can be found in
275 (Solazzo et al., 2011).

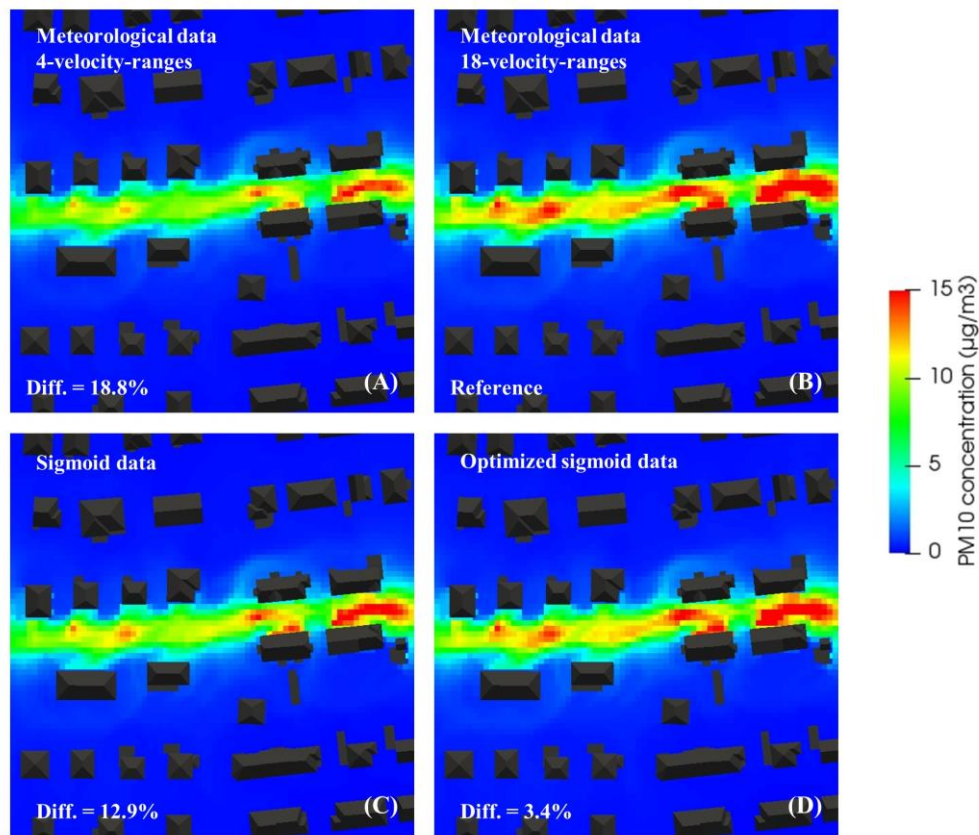
$$276 \quad \bar{C}_d = \frac{\sum_{r=1}^n C_{d,r} \cdot f_{d,r}}{\sum_{r=1}^n f_{d,r}} + C_{bg} \quad (8)$$

$$277 \quad \bar{C} = \frac{\sum_{d=1}^n \bar{C}_d \cdot f_d}{\sum_{d=1}^n f_d} \quad (9)$$

278 where \bar{C}_d is the mean concentration over one wind direction, $C_{d,r}$ is the concentration for a
 279 given wind direction d and a given wind velocity range r , $f_{d,r}$ is the frequency for a given wind
 280 direction and a given wind velocity range, C_{bg} is the background concentration, \bar{C} is the mean
 281 annual concentration and f_d the total frequency of a given wind direction.

282 With this methodology, it is necessary to choose a wind velocity in each velocity range for
 283 which the concentration will be calculated based on the CFD result. A simple choice is to
 284 consider an intermediate velocity, noted v_i , corresponding to the average between the minimal
 285 and the maximal value of the velocity range (e.g., for the velocity range [1.5, 4.5[, the
 286 intermediate value is 3 m/s).

287 A comparison of results for this methodology is given in Fig. 8. with distinct cases considering
 288 (A) the “basic” 4-velocity-range frequencies, (B) the “detailed” 18-velocity-range frequencies,
 289 (C) the frequencies calculated with the sigmoid function, and (D) the frequencies calculated
 290 with the optimized sigmoid function. No background concentration is considered in this study
 291 to permit better comparison of the results.



292

293 Fig. 8. Mean annual concentrations without background concentration based on (A) the “basic” 4-velocity-range monitoring
 294 data, (B) the “detailed” 18-velocity-range monitoring data, (C) the sigmoid interpolation data and (D) the optimized sigmoid
 295 interpolation data.

296 Initially, it can be seen that using the “basic” 4-velocity-range data leads to an underestimation
 297 of the concentrations compared to the case using “detailed” 18-velocity-range data by around
 298 19%. When calculating the “detailed” wind velocity distribution based on the “basic” data with
 299 the sigmoid function, the difference is reduced to 12.9%. Finally, the best results are obtained
 300 when using the optimized sigmoid function with an underestimation of 3.4%. According to
 301 these results, using the “basic” 4-velocity-range frequencies can give an estimation of the mean
 302 annual concentrations but is not sufficient to reach good accuracy compared to the mean annual
 303 concentration calculated with the “detailed” wind velocity distribution. However, using the
 304 sigmoid function and especially the optimized variant significantly improves the results,

305 leading to almost the same results as those obtained with the “detailed” wind velocity
 306 distribution.

307 3.2.2. Discrete methodology with representative velocities

308 The previous methodology used to compute annual concentrations, which was easy to set up,
 309 nonetheless has certain weaknesses that mostly concern the choice of the wind velocity for
 310 which the concentrations will be calculated, based on the CFD results. Using an intermediate
 311 velocity v_i corresponding to the average between the minimal and the maximal value of the
 312 velocity range can lead to underestimations of the mean annual concentrations. Indeed, in doing
 313 so, it is implicitly assumed that the concentration is constant with the wind velocity in a given
 314 wind velocity range. However, according to equation (4), this assumption is wrong because the
 315 concentration evolves hyperbolically with velocity. The representative velocity over one
 316 velocity range, considering the hyperbolic evolution of the concentration, is given in (11) as a
 317 result of (10) and (4).

$$318 \quad \frac{1}{2} \int_{v_{min}}^{v_{max}} c(v) \cdot dv = \int_{v_{min}}^{v_r} c(v) \cdot dv \quad (10)$$

$$319 \quad v_r = \sqrt{\frac{2}{\frac{1}{v_{max}^2} + \frac{1}{v_{min}^2}}} \quad (11)$$

320 where v_{max} and v_{min} are respectively the maximal and the minimal velocities of the velocity
 321 range, v_r is the representative velocity of the velocity range and $c(v)$ the equation describing
 322 the evolution of the concentration as a function of the wind velocity, i.e. equation (4).

323 The representative velocities v_r were calculated with equation (11) and compared to the
 324 intermediate velocities v_i . It is noteworthy that for a velocity range with a minimal velocity of
 325 0 m/s, it is mathematically not possible to compute the representative velocity due to the domain

326 definition of the function. A choice is therefore required; for the purpose of this study, the same
 327 ratio v_r/v_i as for $[0.5, 1.5[$ was considered.

328 According to the results summarized in Table 2. for wind velocities ranging from 0 to 6.5 m/s,
 329 the intermediate velocity can be much higher than the representative velocity for low velocities.
 330 For example, for wind velocities ranging from 0.5 to 1.5 m/s, the intermediate velocity of 1 m/s
 331 is almost twice as high as the representative velocity of 0.67 m/s. For higher velocity ranges,
 332 such as $[2.5, 3.5[$ or more, the differences can be neglected. This last statement is true for 1 m/s
 333 steps between the minimal and the maximal velocities of the velocity range but can become
 334 wrong for higher velocity steps.

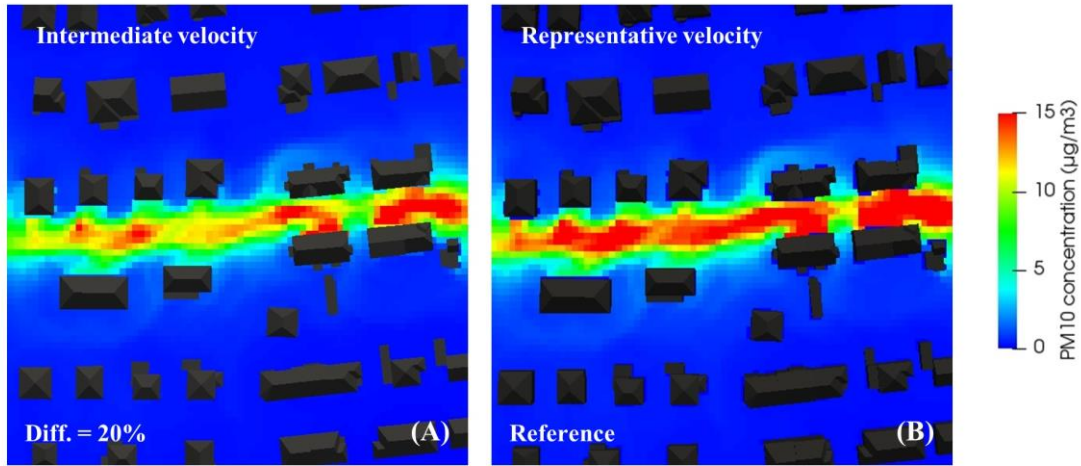
335

336 Table 2. Comparison between the intermediate velocity v_i and the representative velocity v_r (*: the representative velocity was
 337 calculated considering the same ratio v_r/v_i as for $[0.5, 1.5[$).

v_{min} [m/s]	0	0.5	1.5	2.5	3.5	4.5	5.5
v_{max} [m/s]	0.5	1.5	2.5	3.5	4.5	5.5	6.5
v_i [m/s]	0.25	1.00	2.00	3.00	4.00	5.00	6.00
v_r [m/s]	0.1675*	0.67	1.82	2.88	3.90	4.92	5.94
v_r/v_i	0.67*	0.67	0.91	0.96	0.97	0.98	0.99

338

339 Fig. 9. shows a comparison of the mean annual concentrations when using the intermediate
 340 velocity and when using the representative velocity, based on the “detailed” 18-velocity-range
 341 wind distribution. According to the results, using the intermediate velocity leads to considerable
 342 underestimations of the mean annual concentrations compared to the use of the representative
 343 velocity. The underestimation is about 20%. When using the discrete methodology presented
 344 in Section 3.2.1., it is therefore suggested to use the representative velocity instead of the
 345 intermediate velocity to better take into account the hyperbolic evolution of the pollutant
 346 concentrations with the wind velocity to avoid underestimating the concentrations.



347
 348 Fig. 9. Comparison of the mean annual concentrations based on the “detailed” 18-velocity-range wind distribution using (A)
 349 the intermediate velocity and (B) the representative velocity.

350

351 3.2.3. Continuous methodology using the sigmoid function

352 For the last approach, mean annual concentrations based on CFD results can be calculated using
 353 a continuous methodology. This methodology is a combination of equation (4), describing the
 354 evolution of pollutant concentration with wind velocity, and equation (2), describing the
 355 evolution of wind velocity frequency with wind velocity. The equation to compute the mean
 356 annual concentrations continuously is given in (12).

$$357 \quad \bar{C} = \frac{\int_0^{+\infty} c(v) \cdot f(v) \cdot dv}{\int_0^{+\infty} f(v) \cdot dv} + C_{bg} \quad (12)$$

358 where \bar{C} is the mean annual concentration, $c(v)$ is the function describing the evolution of the
 359 concentration with the wind velocity, $f(v)$ is the function describing the evolution of the wind
 360 velocity frequency with the wind velocity, and C_{bg} is the background concentration.

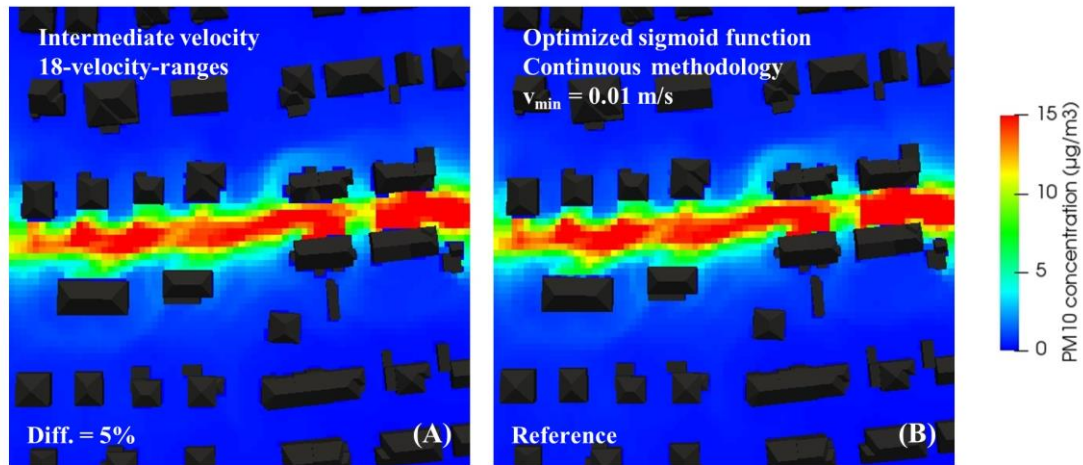
361 Taking equation (4) for $c(v)$ and equation (2) for $f(v)$ leads to a mathematical problem. Indeed,
 362 $c(v)$ is not defined for $v = 0$ and the limit of $c(v) \cdot f(v)$ tends toward infinity when v tends

363 toward 0. To avoid this problem, equation (13) is suggested instead of equation (12). With this
 364 equation, it is considered that a minimal velocity (v_{min}) exists for which the pollutant
 365 concentration will no longer increase when the wind velocity decreases. This hypothesis can be
 366 justified by the additional effects, such as traffic-induced turbulence (Vachon et al., 2002) and
 367 atmospheric stability (Qu et al., 2012) that may participate in pollutant dispersion for low wind
 368 velocities or become preponderant. We suggest applying a constant pollutant concentration for
 369 wind velocities ranging from 0 to v_{min} and suggest using $C_{max} = c(v_{min})$. The choice of v_{min}
 370 is particularly important when using the optimized sigmoid function.

$$371 \quad \bar{C} = C_{max} \cdot \frac{\int_0^{v_{min}} f(v) \cdot dv}{\int_0^{+\infty} f(v) \cdot dv} + \frac{\int_{v_{min}}^{+\infty} c(v) \cdot f(v) \cdot dv}{\int_0^{+\infty} f(v) \cdot dv} + C_{bg} \quad (13)$$

372 where \bar{C} is the mean annual concentration, C_{max} is the maximal concentration accepted for the
 373 calculation, v_{min} is the velocity under which $c(v)$ is considered equal to C_{max} , $f(v)$ is equation
 374 (2), $c(v)$ is equation (4) and C_{bg} is the background concentration.

375 Fig. 10. shows a comparison between the discrete methodology with the representative
 376 velocities and the continuous methodology using the optimized sigmoid function. It can be seen
 377 that the results of the discrete methodology given in Fig. 10. (A) can be reached by the
 378 continuous methodology. Nonetheless, the difference of 5% reached using $v_{min} = 0.01$ m/s can
 379 increase when changing the value of v_{min} : lower values will lead to higher concentrations
 380 whereas higher values will lead to lower concentrations. The value of v_{min} must therefore be
 381 chosen carefully.



382

383 Fig. 10. Comparison of the mean annual concentrations (A) based on the “detailed” 18-velocity-range wind distribution and
 384 using the intermediate velocity, and (B) based on the optimized sigmoid function and $v_{min} = 0.01$ m/s.

385 4. Discussion

386 This study provides tools to assess wind velocity distributions based on “basic” data and mean
 387 annual air pollutant concentrations based on CFD results. Additional work should be done to
 388 improve the methodologies and the major issues are discussed hereafter.

389 The capability of the Weibull and the sigmoid functions to describe wind velocity distribution
 390 was assessed based on wind data from four meteorological stations in France. All of these
 391 stations were located in peri-urban environments close to large French cities. It is necessary to
 392 take into account that the results, and especially the interpolation-related errors, might be
 393 different for other types of stations such as urban and rural stations, and for other countries with
 394 different wind characteristics. In particular, the optimization suggested for the sigmoid function
 395 may not be suitable for different countries or type of station. Further works are therefore
 396 required in this direction.

397 The mean annual atmospheric pollutant concentrations can be calculated using a discrete
 398 methodology. However, this methodology has two major problems. The first concerns the
 399 choice of wind velocity for which the pollutant concentrations will be calculated: choosing an

400 intermediate velocity is a simple approach which can lead to considerable underestimations of
401 pollutant concentrations, and it is better to use a representative velocity instead, as suggested in
402 this paper. Using the representative velocity requires, however, making a choice for the first
403 velocity range. The second problem concerns the velocity step used to build the wind velocity
404 ranges: the result depends on the velocity step used, especially for the lower wind velocities for
405 which a decrease in the velocity-step leads to higher mean annual concentrations. To avoid
406 these two problems, a continuous methodology has been proposed. This methodology does not
407 have an intrinsic limitation, but dependent on the function describing the evolution of the
408 concentration as a function of wind velocity. If we consider a hyperbolic evolution of the
409 concentration with wind velocity, it is necessary to choose a minimal value of velocity for which
410 it is considered that lower velocities will not increase the concentrations due to compensatory
411 phenomena (traffic-induced turbulence, atmospheric stability, etc.). The value of the minimal
412 velocity is open to discussion and assessing this value is outside the scope of this paper. Further
413 works are required, for example with infield measurement campaigns and comparisons between
414 mean annual concentrations monitored and calculated with the continuous methodology.

415 Finally, it should be noted that the methodologies to assess mean annual concentrations were
416 addressed using CFD results implying a neutral atmosphere, but can be used for any numerical
417 results as long as a function describing the evolution of the concentration with the wind velocity
418 is available.

419

420

421 **5. Conclusion**

422 The objectives of this study were to provide methodologies; (1) to assess wind velocity
423 distribution based on “basic” data, and (2) to assess mean annual air pollutant concentrations

424 based on numerical results. Three approaches for each objective were described and compared
425 throughout this paper and the main conclusions are as follows:

426 (1.a) The Weibull distribution and the sigmoid function can both accurately reproduce
427 “detailed” 18-velocity-range wind distribution based on “basic” 4-velocity-range wind
428 data with an average error of 12%. These functions can nonetheless underestimate the
429 frequencies of low velocities.

430 (1.b) The optimized sigmoid function improves the wind distribution results over the
431 standard sigmoid function, especially for low wind velocities.

432 (2.a) Using “basic” 4-velocity-range wind data and the discrete methodology can provide an
433 estimation of the mean annual concentrations but is not sufficient to achieve high
434 precision, leading to a difference of around 19% compared to the use of “detailed”
435 18-velocity-range wind data. Using the sigmoid function instead, based on the “basic”
436 wind data improves the mean annual concentration results with a global error of less
437 than 4%.

438 (2.b) When using the discrete methodology to assess mean annual concentrations, it is
439 suggested to use a representative velocity of the function describing the evolution of
440 pollutant concentrations with the wind velocities instead of an intermediate velocity.
441 The intermediate velocity leads to underestimations of mean annual concentrations,
442 especially when using CFD results with a neutral case hypothesis where the
443 concentration evolves hyperbolically with the wind velocity.

444 (2.c) Mean annual concentrations can be assessed using a continuous methodology that does
445 not have any of the limitations of discrete methodologies. It is, however, limited by
446 the function describing the evolution of the concentrations with the wind velocities,
447 which leads to the need to choose a minimal velocity when using the sigmoid function.

448 Finally, the methodologies presented in this paper can be used for outdoor air quality study
 449 purposes, which is a relevant starting point for improving both outdoor and indoor air quality
 450 and, therefore, a key-point to achieve smart sustainable cities.

451

452 **Acknowledgments**

453 We would like to thank the ANRT (Association Nationale de la Recherche et de la Technologie)
 454 for their support and Météo-France for allowing us to use their data for this study.

455

456 **References**

- 457 Anderson, J.O., Thundiyil, J.G., Stolbach, A., 2012. Clearing the Air: A Review of the Effects
 458 of Particulate Matter Air Pollution on Human Health. *J. Med. Toxicol.* 8, 166–175.
 459 <https://doi.org/10.1007/s13181-011-0203-1>
- 460 Bai, L., He, Z., Li, C., Chen, Z., 2020. Investigation of yearly indoor/outdoor PM_{2.5} levels in
 461 the perspectives of health impacts and air pollution control: Case study in Changchun,
 462 in the northeast of China. *Sustainable Cities and Society* 53, 101871.
 463 <https://doi.org/10.1016/j.scs.2019.101871>
- 464 Bibri, S.E., Krogstie, J., 2017. Smart sustainable cities of the future: An extensive
 465 interdisciplinary literature review. *Sustainable Cities and Society* 31, 183–212.
 466 <https://doi.org/10.1016/j.scs.2017.02.016>
- 467 Blocken, B., 2015. Computational Fluid Dynamics for urban physics: Importance, scales,
 468 possibilities, limitations and ten tips and tricks towards accurate and reliable
 469 simulations. *Building and Environment* 91, 219–245.
 470 <https://doi.org/10.1016/j.buildenv.2015.02.015>
- 471 Buccolieri, R., Santiago, J.-L., Rivas, E., Sanchez, B., 2018. Review on urban tree modelling
 472 in CFD simulations: Aerodynamic, deposition and thermal effects. *Urban Forestry &
 473 Urban Greening* 31, 212–220. <https://doi.org/10.1016/j.ufug.2018.03.003>
- 474 Chaloulakou, A., Mavroidis, I., Gavriil, I., 2008. Compliance with the annual NO₂ air quality
 475 standard in Athens. Required NO_x levels and expected health implications.
 476 *Atmospheric Environment* 42, 454–465.
 477 <https://doi.org/10.1016/j.atmosenv.2007.09.067>

- 478 EU, 2008. Directive 2008/50/EC of the european parliament and of the council of 21 May 2008
479 on ambient air quality and cleaner air for Europe, European Union.
- 480 Franke, J., Hellsten, A., Schlünzen, H., Carissimo, B., 2007. Best practice guideline for the
481 CFD simulation of flows in the urban environment. COST Action 732.
- 482 Jenkin, M.E., 2004. Analysis of sources and partitioning of oxidant in the UK—Part 1: the
483 NOX-dependence of annual mean concentrations of nitrogen dioxide and ozone.
484 Atmospheric Environment 38, 5117–5129.
485 <https://doi.org/10.1016/j.atmosenv.2004.05.056>
- 486 Jurado, X., Reiminger, N., Vazquez, J., Wemmert, C., Dufresne, M., Blond, N., Wertel, J.,
487 2020. Assessment of mean annual NO₂ concentration based on a partial dataset.
488 Atmospheric Environment 221, 117087.
489 <https://doi.org/10.1016/j.atmosenv.2019.117087>
- 490 Kim, K.-H., Kabir, E., Kabir, S., 2015. A review on the human health impact of airborne
491 particulate matter. Environment International 74, 136–143.
492 <https://doi.org/10.1016/j.envint.2014.10.005>
- 493 Kumar, M.B.H., Balasubramanian, S., Padmanaban, S., Holm-Nielsen, J.B., 2019. Wind
494 Energy Potential Assessment by Weibull Parameter Estimation Using Multiverse
495 Optimization Method: A Case Study of Tirumala Region in India. Energies 12, 2158.
496 <https://doi.org/10.3390/en12112158>
- 497 Mahmood, F.H., Resen, A.K., Khamees, A.B., 2019. Wind characteristic analysis based on
498 Weibull distribution of Al-Salman site, Iraq. Energy Reports S2352484719308716.
499 <https://doi.org/10.1016/j.egy.2019.10.021>
- 500 Qu, Y., Milliez, M., Musson-Genon, L., Carissimo, B., 2012. Numerical study of the thermal
501 effects of buildings on low-speed airflow taking into account 3D atmospheric radiation
502 in urban canopy. Journal of Wind Engineering and Industrial Aerodynamics 104–106,
503 474–483. <https://doi.org/10.1016/j.jweia.2012.03.008>
- 504 Reiminger, N., Vazquez, J., Blond, N., Dufresne, M., Wertel, J., 2020. CFD evaluation of mean
505 pollutant concentration variations in step-down street canyons. Journal of Wind
506 Engineering and Industrial Aerodynamics 196, 104032.
507 <https://doi.org/10.1016/j.jweia.2019.104032>
- 508 Richards, P.J., Norris, S.E., 2011. Appropriate boundary conditions for computational wind
509 engineering models revisited. Journal of Wind Engineering and Industrial
510 Aerodynamics 99, 257–266. <https://doi.org/10.1016/j.jweia.2010.12.008>
- 511 Santiago, J.-L., Buccolieri, R., Rivas, E., Sanchez, B., Martilli, A., Gatto, E., Martín, F., 2019.
512 On the Impact of Trees on Ventilation in a Real Street in Pamplona, Spain. Atmosphere
513 10, 697. <https://doi.org/10.3390/atmos10110697>

- 514 Schatzmann, M., Leitl, B., 2011. Issues with validation of urban flow and dispersion CFD
515 models. *Journal of Wind Engineering and Industrial Aerodynamics* 99, 169–186.
516 <https://doi.org/10.1016/j.jweia.2011.01.005>
- 517 Ścibor, M., Balcerzak, B., Galbarczyk, A., Targosz, N., Jasienska, G., 2019. Are we safe inside?
518 Indoor air quality in relation to outdoor concentration of PM10 and PM2.5 and to
519 characteristics of homes. *Sustainable Cities and Society* 48, 101537.
520 <https://doi.org/10.1016/j.scs.2019.101537>
- 521 Shaw, C., Boulic, M., Longley, I., Mitchell, T., Pierse, N., Howden-Chapman, P., 2020. The
522 association between indoor and outdoor NO2 levels: A case study in 50 residences in
523 an urban neighbourhood in New Zealand. *Sustainable Cities and Society* 56, 102093.
524 <https://doi.org/10.1016/j.scs.2020.102093>
- 525 Solazzo, E., Vardoulakis, S., Cai, X., 2011. A novel methodology for interpreting air quality
526 measurements from urban streets using CFD modelling. *Atmospheric Environment* 45,
527 5230–5239. <https://doi.org/10.1016/j.atmosenv.2011.05.022>
- 528 Toparlar, Y., Blocken, B., Maiheu, B., van Heijst, G.J.F., 2017. A review on the CFD analysis
529 of urban microclimate. *Renewable and Sustainable Energy Reviews* 80, 1613–1640.
530 <https://doi.org/10.1016/j.rser.2017.05.248>
- 531 Vachon, G., Louka, P., Rosant, J.-M., Mestayer, P.G., Sini, J.-F., 2002. Measurements of
532 Traffic-Induced Turbulence within a Street Canyon during the Nantes'99 Experiment,
533 in: Sokhi, R.S., Bartzis, J.G. (Eds.), *Urban Air Quality — Recent Advances*. Springer
534 Netherlands, Dordrecht, pp. 127–140. https://doi.org/10.1007/978-94-010-0312-4_10
- 535 Vranckx, S., Vos, P., Maiheu, B., Janssen, S., 2015. Impact of trees on pollutant dispersion in
536 street canyons: A numerical study of the annual average effects in Antwerp, Belgium.
537 *Science of The Total Environment* 532, 474–483.
538 <https://doi.org/10.1016/j.scitotenv.2015.06.032>
- 539 Wang, P., Zhao, D., Wang, W., Mu, H., Cai, G., Liao, C., 2011. Thermal Effect on Pollutant
540 Dispersion in an Urban Street Canyon. *International Journal of Environmental Research*
541 5, 813–820. <https://doi.org/10.22059/ijer.2011.388>
- 542 WHO, 2017. Evolution of WHO air quality guidelines past, present and future, Copenhagen:
543 WHO Regional Office for Europe.
- 544 Yang, J., Shi, B., Shi, Y., Marvin, S., Zheng, Y., Xia, G., 2020. Air pollution dispersal in high
545 density urban areas: Research on the triadic relation of wind, air pollution, and urban
546 form. *Sustainable Cities and Society* 54, 101941.
547 <https://doi.org/10.1016/j.scs.2019.101941>

548